We are IntechOpen, the world's leading publisher of Open Access books Built by scientists, for scientists

4,800
Open access books available

122,000
International authors and editors

135M
Downloads

Our authors are among the

154
Countries delivered to

TOP 1%
most cited scientists

12.2%
Contributors from top 500 universities

CLARIVATE ANALYTICS BOOK CITATION INDEX INDEXED

WEB OF SCIENCE™

Selection of our books indexed in the Book Citation Index in Web of Science™ Core Collection (BKCI)

Interested in publishing with us?
Contact book.department@intechopen.com

Numbers displayed above are based on latest data collected.
For more information visit www.intechopen.com

Chapter 4

Numerical Analysis and Experimental Investigation of Energy Partition and Heat Transfer in Grinding

Lei Zhang

Additional information is available at the end of the chapter

http://dx.doi.org/10.5772/52999

1. Introduction

In industry, structural parts have to be subjected to a heat treatment to increase fatigue strength or wear resistance of the surface layers and to adjust special combinations of material properties, which strengthen the surface layer of components and consequently improve the load capacity and lifetime. The heat treatment processes of the surface layer are some typical advantages compared to the full hardening heat treatments (Zhang 2004). In industry various heat treatment methods are used for the production of required surface layer properties. But these processes cannot simply be integrated into the production line because of economical disadvantage. A new technology called grind-hardening can utilize the grinding heat for martensitic phase transformation of the work piece surface layer (Brinksmeier and Brockhoff 1996; Brockhoff 1999). In contrast to conventional grinding processes, grind-hardening is based on extensive heat generation in the contact zone between grinding wheel and workpiece causing the austenitizing the surface layer material. The martensitic hardening is usually achieved by self-quenching mechanisms. Metallurgic investigations as well as hardness and residual stress measurements confirmed the possibility and the potential of this new heat treatment method, which can be integrated into existing production lines to decrease manufacturing cost, improve machining efficiency and reduce production time (Zarudi and Zhang 2002).

Fundamental investigations were carried out to determine the basic mechanisms of the short-time metallurgical processes, as well as the influence of the process parameters on the hardening result. The properties of the grind-hardened surface layers were evaluated by residual stress measurements and metallographic analyses as well as hardness measurement (Zarudi and Zhang 2002; Liu and Wang 2004; Wang and Liu 2005). Due to the process kinematics, grind-hardening is classified as a short-time heat treatment. Particularly in

short-time heat treatments, composition and initial structural state of the material have an important influence on the hardening result. For grind-hardening the same mechanisms as for conventional heat treatments were verified. The hardening result depends on the content of carbon and alloying elements, as well as on the distribution of carbon at the initial materials state. High hardness penetration depths were obtained with tempered alloyed hyper-and hypo-eutectoid steels (Liu and Wang 2004).

Besides the material composition and initial state, as well as the grinding wheel specification, the parameters of the grind-hardening process also significantly influence the hardening result. The cut depth has the most important influence on the result of the grind-hardening operation. With increasing cut depth the cutting power and the generated heat increase. Thus the hardness penetration depth rises with increasing cut depth (Liu and Wang 2005). The interrelation of the table speed and the hardening result is more complex, because the table speed influences two factors that are highly important for the material phase transformation. With increasing table speed the cutting power and the heat quantity increases. Also the duration of the heat impact decreases with increasing table speed. Thus the table speed has to be adjusted to generate high heat quantities and sufficient heating durations. Concerning the cutting speed basic investigations did not prove a definite influence on the hardness penetration depth (Brinksmeier and Brockhoff 1996).

Most of analytical thermal models are based on the early work by Jaeger, where the grinding wheel is represented by a heat source, equally distributed over the contact length between the workpiece and the grinding wheel, moving along the surface of the workpiece with a speed equal to the speed of workpiece (Jaeger 1942; Rowe and Jin 2001; Ramesh et al. 1999; Lavine 2000). In grinding the total grinding energy is distributed not only in the workpiece but also in the grinding wheel, the chip, and the coolant. A prediction of these energy components and the effect of cooling, along with the various assumptions made, related to the thermal prosperities of the workpiece material and the exact heat source profile have been made in order to improve the simulation model (Zhang 2004; Zhang 2005).

The finite element method has been used for modelling the grinding process, which allows for the calculation of the grinding temperatures and their distribution within the workpiece, in order to achieve a greater accuracy and more reliable results. Experiment was performed with the different conditions. Semi-natural thermocouple is used to measure the temperature field of surface layer in grinding. The maximal surface temperature and the temperature field in the surface layer of the workpiece during grinding can be theoretically predicted by using the finite element model.

In grinding process almost all the grinding energy is converted into heat within a small grinding zone. A large part of the generated heat flows into the workpiece, which results in extremely high temperature at the interface between the wheel and the workpiece. This can cause elevated temperatures and harden layer of the work piece. Analysis of the grinding temperature requires detailed knowledge about the grinding energy, heat flux distribution along the grinding zone, the fraction transported as heat to the workpiece, and cooling by the applied fluid. In order to calculate the temperature, it is necessary to specify the energy partition within the workpiece.

One approach to estimate the energy partition within the workpiece is fitting the subsurface temperature respond to analytically calculated values. The energy partition is obtained using temperature matching and inverse heat transfer methods. The temperature response in the workpiece subsurface can be measured during straight surface plunge using an embedded thermocouple. With each grinding pass, the temperature response is measured closer to the surface being ground. Another approach for analyzing the energy partition is the single grain model. This model includes the effects of heat transfer to the abrasive grains, fluid, and work piece by considering a single grain surrounded by fluid interacting with the workpiece. Each single active grain is modeled as a truncated cone moving along the workpiece surface at the wheel speed with all of the grinding energy uniformly dissipated at the grain and workpiece interface area. Cooling by the fluid is then taken into account by considering the temperature at the fluid-workpiece interface within the grinding zone, but the convective coefficient is difficult to calculate. In order to solve the problem, a composite model is analyzed. It assumes that the surface porosity is completely filled with grinding fluid and that the thermal properties of the composite can be approximated by a weighted volumetric average of the thermal properties of the grain and grinding fluid. Some energy would be carried away with the grinding chips, but this is usually negligible in energy partition model.

In order to estimate the energy partition within the workpiece, an integral approximation solution of energy partition is studied to calculate the energy partition within the work piece, wheel, chip and fluid in the grinding process. Heat transfer models of the abrasive grain, workpiece, chips and fluid were analyzed by using the integral approximation method. The present model can calculate the energy partition with and without film boiling in the grinding zone. Experiments were performed with the different grinding conditions. Semi-natural thermocouple is used to measure the temperature field of steel surface layer in grinding. Temperature field of alloy steel is simulated by finite element method. The workpiece background temperature calculated by the present model agreed very well with the experimental results. Energy partition model can be used to calculate the grinding temperature for controlling thermal damage and predicting the harden layer depth in grinding.

2. Thermal principle

The following describes developments achieved over more than twenty years of research. The approach developed by the author and his colleagues has been influenced by many previous workers whose achievements are acknowledged. The most recent revised approach is the result of many refinements and experiments undertaken to achieve generality for all grinding processes.

2.1. Heat flows

In grinding, there are four kinds of heat flows. Heat flows to the workpiece, to the abrasive grains, to the grinding fluid and into the chips. If it assumed that all heat goes into the

workpiece, temperatures predicted are much too high. In many cases the workpiece would completely melt. However, if heat flows to the wheel, chips and fluid are subtracted from the total heat, the maximum workpiece temperature can be simply estimated. There is a special case where ignoring heat to the wheel, chips and fluid is reasonable but over-estimates workpiece temperatures. The over-estimate is typically about a third. This special case is for dry shallow-cut grinding steels and cast irons with conventional abrasives at high values of specific energy. However, simple techniques have been developed to take account of the four kinds of heat flows. The approach becomes very general and applies for all grinding situations including low specific energies, creep-feed grinding and HEDG. This has been demonstrated by numerous case studies. Super-abrasives, easy-to-grind materials and deep cuts make the general approach absolutely essential.

2.2. Workpiece heat transfer

An early assumption was that heat was generated at the shear plane. However, the main source of heat in grinding was shown to be the grain-workpiece rubbing surface. In either case, temperatures must be solved using the theory of moving heat sources. A sliding heat source solution applies for shallow-cut grinding. An oblique heat source solution applies for both shallow-cut and deep grinding [Rowe 2001]. Although the oblique heat source solution is a large improvement on the Jaeger sliding heat source and is accurate for shallow cuts, for deep cuts, it slightly over-estimates maximum contact-surface temperatures. A circular arc heat source solution extended the oblique heat source approach [Rowe and Jin 2001]. The circular arc heat source data presented in this chapter has been re-computed and provides better accuracy than the oblique heat source.

2.3. Fluid convection

For shallow grinding, convective cooling occurs mainly outside the contact region. However, it is cooling within the contact region that prevents thermal damage and therefore it is necessary to make this distinction as in the approach outlined below. Much greater fluid cooling takes place inside the grinding contact with deep cuts. This is due to the large contact length in deep grinding. Usually in creep-feed grinding, most of the heat goes to the fluid. The energy which may be extracted is limited by fluid boiling. This was confirmed for shallow grinding. Measurements show that effective cooling techniques can produce very high fluid convection factors within the grinding contact area.

2.4. Chip energy

The energy q_{ch} carried away by the chips is strictly limited but can easily be estimated. The limit is the energy that causes melting. There is also a small amount of kinetic energy that can easily be shown to be negligible. It is known that chips do not usually melt before being detached. For ferrous materials, the maximum energy carried within the chips is approximately 6 J/mm^3 of material removed.

2.5. Heat partitioning

Heat partition is the process of sharing out the four kinds of heat flows to determine the heat into the workpiece.

- **The work partition ratio R_w:** R_w defines the net heat entering the workpiece where $R_w = q_w/q$. Typically, R_w may be as low as 5% in deep grinding or as high as 75% in conventional grinding.
- **The work-wheel fraction R_{ws}:** Some heat q_{ch} is carried away by the chips. The remaining heat $q - q_{ch}$ is shared between the wheel and the workpiece at the grain contacts. In short, $q - q_{ch} = q_s + q_{wg}$. Initially, heat q_{wg} goes into the workpiece but this heat is larger than the net heat into the workpiece q_w. This is because some heat immediately comes out from the workpiece again into the fluid. Therefore, the net heat flow into the workpiece q_w is less than q_{wg}. In other words: $q_{wg} = q_w + q_f$. The work-wheel fraction is $R_{ws} = q_{wg} / (q_s + q_{wg})$. The work-wheel fraction for conventional abrasives is of the order of 85% and for super-abrasives of the order of 50%.
- **Heat to the wheel:** Heat shared between the workpiece and the wheel yields the heat conducted into the wheel. Two different approaches have been employed: Wheel contact analysis and grain contact analysis.

2.6. Wheel contact analysis

An early technique was later abandoned for practical reasons. The early technique estimated the work-wheel fraction based on the thermal properties and speeds of the wheel and the workpiece using the expression $\sqrt{\beta_s v_s / \beta_w v_w}$ (Marinescu 2004). However, bulk thermal properties for the wheel are required and are not available from published data. This technique was later abandoned in favor of the grain contact analysis.

2.7. Grain contact analysis

A grain contact model allows the work-wheel fraction to be based on grain properties rather than bulk wheel properties. A good case can be made that grain properties are physically more relevant than bulk wheel properties since heat partition takes place at the grains. Initially, the conical grain model by Lavine (Lavine et al 1989) was incorporated within our heat partition approach. At the same time, a plane grain solution had been derived for comparison. (Rowe et al 1991) The plane grain model was found to be more accurate than the conical model (Rowe et al 1997). It was realized later that the steady-state version of our plane grain model only differed in minor detail from a very early steady-state assumption. In most cases, a steady-state model is sufficiently accurate. However, the plane grain model can be readily extended to a more accurate transient solution when required.

2.8. Heat input

Grinding power goes into the contact zone as heat. A negligible proportion accelerates the chips and a very small proportion is locked into the deformed material. Power per unit area

is known as heat flux q. The heat is divided by the real contact length and the width of the grinding contact. $q = P/l_c.b_w$

- **Flash heating:** Heat enters the grinding contact in short bursts of intensive energy leading to flash temperatures. The flash temperatures occur in the extremely short time it takes for a grain to pass a point on the workpiece. A point on the workpiece has contact with an individual grain for approximately 1 micro-second. The heat enters the contact in a near-adiabatic process.
- **Grain heating:** A grain is heated at the grain-workpiece contact for much longer than a point on the workpiece. A grain typically moves across the whole contact length in 100 micro-seconds. The grain therefore experiences a heat pulse for a period approximately 100 times longer than a point on the workpiece. It can be shown that this allows the surface of the grain to reach quasi steady-state temperatures. The maximum grain temperature is close to the workpiece melting temperature.
- **Background heating:** Numerous flash contacts gradually heat up the whole workpiece contact area. It is usual therefore to make a distinction between flash temperatures at a grain contact and background temperatures over the whole contact area. The overall duration of energy pulses in the contact area that provides the background temperatures is of the order of 10,000 micro-seconds. This is the time it takes the wheel to move through the contact length. Many energy pulses lead to background temperature rise at depths up to and often exceeding1 mm.

3. Energy partition

An integral approximation solution of energy partition is studied in the grinding process. Flux into the chips was estimated from the limiting chip energy to raise the chip material close to melting.

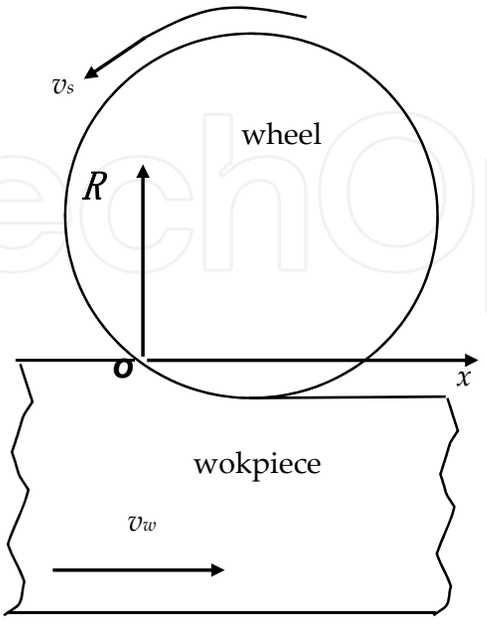

Figure 1. Coordinate system of grinding

The physical model and the coordinate system for a typical grinding wheel and workpiece are shown in Fig. 1. The total heat flux on the contact area of wheel and workpiece is qn(x). Therefore,

$$q_n(x) = q_{wh}(x) + q_{wb}(x) + q_f(x) + q_{ch}(x) \tag{1}$$

Where, $q_{wh}(x)$, $q_{wb}(x)$, $q_f(x)$ and $q_{ch}(x)$ are the heat fluxes into the grinding wheel, workpiece, fluid and chips, respectively as shown in Fig.2. Flux into the chips was estimated from the limiting chip energy to raise the chip material close to melting. Taking the mean value of specific heat from ambient temperature to melting point (about 1500℃), the partial limiting chip energy, e_{ch}, flows into workpiece material. Therefore

$$q_{ch} = e_{ch} a v_w / l_c \tag{2}$$

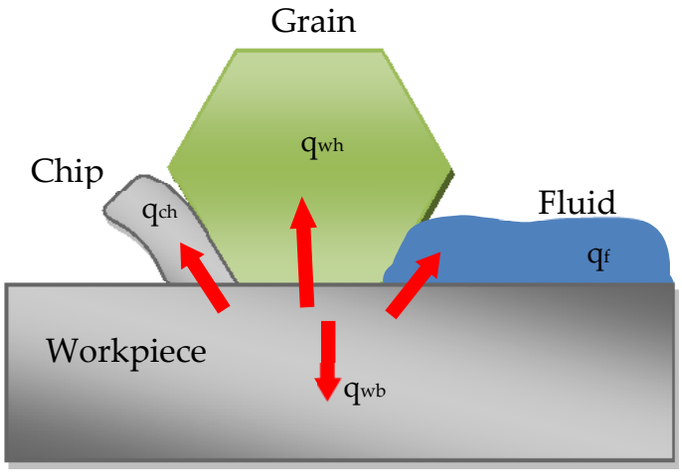

Figure 2. Heat flows to the workpiece, the grain, the chip and the fluid

Many grains of the wheel surface cut into the workpiece with a very high speed and a lot of heat is generated in the grain-workpiece interface. The heat generated at the grain-workpiece interface, ql(x), is assumed to be uniform in the present study, and will conduct into the workpiece and grain. Therefore

$$q_l(x) = q_g(x) + q_{wg}(x) \tag{3}$$

Where, $q_g(x)$ and $q_{wg}(x)$ are the heat fluxes into the grain and workpiece. The ratio between real contact area A_r of grain-workpiece and geometric contact area A_n of wheel-workpiece is A, then

$$q_l(x) = q_n(x)\frac{A_n}{A_r} = \frac{q_n(x)}{A} \tag{4}$$

The heat flux into the workpiece $q_{wg}(x)$ will be divided into three parts. First part remains in the workpiece, second part conducts into fluid, and third part is removed by chips, then

$$q_{wg}(x)A_r = q_{wb}(x)A_n + q_f(x)(A_n - A_r) + q_{ch}(x)A_n \tag{5}$$

For Ar<<An, from formula (3) and (5), then

$$q_l(x)A = q_g(x)A + q_{wb}(x) + q_f(x) + q_{ch}(x) \tag{6}$$

It is assumed that the grinding fluid fills the space around the abrasive grain to a depth that is larger than the thickness of the thermal boundary layer. Therefore, the grinding fluid flow over the workpiece surface can be considered as slug flow with grinding velocity vs. Finally, the grinding fluid can be modeled as a moving semi-infinite solid with a variable heat flux q_f (x) at its surface. The temperature, T_f, of the grinding fluid can be obtained by using an integral approximation solution,

$$T_f = \left[\frac{4}{3\left(K\rho C\right)_f (v_s \pm v_w) q_f(x)} \int_0^x q_f(x)dx \right]^{\frac{1}{2}} q_f(x) \tag{7}$$

Since the workpiece moves with table velocity, v_w, the heat transfer into the workpiece background can be considered as a heat conduction problem in a moving semi-infinite solid. Therefore, the background temperature, T_{wb}, of the workpiece can be expressed as

$$T_{wb} = \left[\frac{4}{3\left(K\rho C\right)_{wb} v_w q_{wb}(x)} \int_0^x q_{wb}(x)dx \right]^{\frac{1}{2}} q_{wb}(x) \tag{8}$$

The temperature distribution in the grain is assumed to be a cubic polynomial function. The grain temperature, Tg, at the grain-workpiece surface can be expressed as

$$T_g = \frac{r_0}{K_g} \frac{\eta}{\eta + 3} q_g(x) \tag{9}$$

An individual grain is modelled as a band heat source with width l_g, causing a heat flux q_{wg}(x) into workpiece surface. The average workpiece surface temperature, T_{wg}, underneath a grain due to an individual heat source can be expressed as

$$T_{wg} = \frac{4}{3}\left[\frac{l_g}{\pi\left(K\rho C\right)_{wb} (v_s \pm v_w)} \right]^{\frac{1}{2}} q_{wg}(x) \tag{10}$$

In grinding arc area, the energy partition must satisfy the compatibility requirement that the temperature on the workpiece surface equals the temperature on the grain and fluid surface everywhere along the grinding zone. Therefore,

$$T_f = T_{wb} \tag{11}$$

$$T_g = T_{wb} + T_{wg} \tag{12}$$

From the formula (1) to (12), energy partition of chips, work piece, fluid and wheel can be expressed as

$$R_{ch} = \frac{e_{ch} a v_w b}{F_t v_s} \tag{13}$$

$$R_{wb} = \frac{N}{(1+U)(G+N)+WA}(1-R_{ch}) \tag{14}$$

$$R_f = \frac{q_f}{q_n} = \frac{NU}{(1+U)(G+N)+WA}(1-R_{ch}) \tag{15}$$

$$R_{wh} = \frac{q_{wh}}{q_n} = \frac{G(1+U)+WA}{(1+U)(G+N)+WA}(1-R_{ch}) \tag{16}$$

And

$$N = \frac{l_g}{\sqrt{\pi} K_g} \frac{\eta}{\eta+3} \tag{17}$$

$$W = \left[\frac{4}{3(K\rho C)_{wb} v_w q_{wb}(x)} \int_0^x q_{wb}(x) dx \right]^{\frac{1}{2}} \tag{18}$$

$$U = \left[\frac{(K\rho C)_f (v_s \pm v_w)}{(K\rho C)_{wb} v_w} \right]^{\frac{1}{2}} \tag{19}$$

$$G = \frac{2}{3} \left[\frac{4 l_g}{\pi (K\rho C)_{wb} (v_s \pm v_w)} \right]^{\frac{1}{2}} \tag{20}$$

4. Numerical simulation

4.1. Finite element model

The finite element model proposed here is based on Jaeger's model. Grinding heat is entering the workpiece on the top surface of the work piece, in the form of heat flux q, input that moves along this surface. All the other sides of the work piece are considered to be adiabatic, and so no heat exchange takes place in these sides. The model has a length of

26mm and a height of 10mm, sufficient enough for the temperature fields to be fully deployed and observed in full length. A mesh method is applied on the proposed model, consisting of 2400 4-noded quadrilateral elements and 1501 nodes, as shown in Fig. 3.

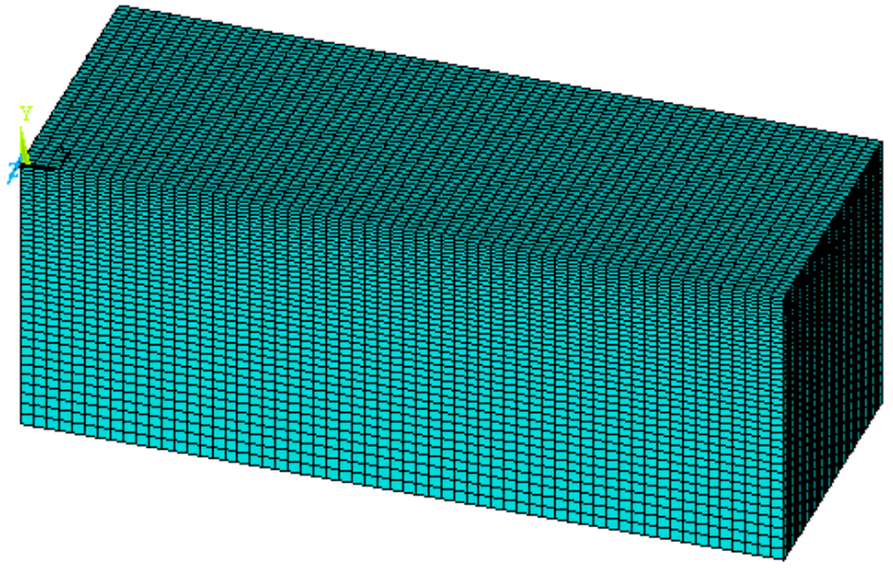

Figure 3. The meshed workpiece model

The mesh grid is denser towards the grinding surface, which is the thermally loaded surface, and, thus the most affected zone of the workpiece, allowing for greater accuracy to be obtained.

4.2. Grinding contact length

For the proposed model, except the work conditions and the material prosperities, contact length need to be calculated in order to determine the temperatures. The geometrical contact length between the workpiece and the grinding wheel is equal to

$$l_c^2 = l_f^2 + l_g^2 \tag{21}$$

Where l_f is the contact length between surfaces acted on by a normal force and l_g is the geometric contact length defined by Equation (21). The length l_f is evaluated from:

$$l_f = \sqrt{8F_n^{'}(Ks + Kw)d_s} \tag{22}$$

Where $F_n^{'}$ is the specific normal force, and

$$Ks = \frac{1-\nu_s^2}{\pi E_s} \tag{23}$$

$$Kw = \frac{1-\nu_w^2}{\pi E_w} \tag{24}$$

Variables Ks and Kw are determined from the physical properties of materials in the contact. ν_s and ν_w are Poisson's ratios, E_s and E_w are the Young's Modulus. The real contact length can be expressed using a surface roughness approach or a contact area approach. The first yields more faithful results in comparison with the experimental results. Based on the roughness approach, the magnitude of the grinding contact length is represented as：

$$l_c = \sqrt{(l_{fr})^2 + l_g^2} = \sqrt{(R_r l_f)^2 + l_g^2} \tag{25}$$

Where l_{fr} is contact length for rough surfaces with normal force and R_r is roughness factor. The magnitudes of the roughness factor are acquired as experimental values from the tests. R_r is sensitive to the grinding conditions for some material combinations. For general analysis of the grinding conditions, where measured values of the roughness factor are not available, it is suggested that the value R_r is equal 8.

Combining equations (21), (22) and (25) yields the relationship

$$l_c = \sqrt{8R_r{}^2 F_n^{'}(Ks + Kw)d_s + ad_s} \tag{26}$$

Where a is the depth of cut and ds the diameter of the grinding wheel. Equation (26) determines the contact length between the wheel body and workpiece taking account not only elastic deflection and geometric effect but also roughness of both surfaces in the contact.

4.3. Heat flux profile

The heat flux q, that is distributed over the contact length can be calculated as

$$q = R_w \frac{F_t v_s}{b l_c} s(x) \tag{27}$$

where F_t is the tangential force, v_s is the wheel speed, b is the grinding width, and R_w is the heat partition of the energy entering the work piece. This kind of modelling is suitable for a grinding process with a very small depth of cut, since there is no modelling of the chip. The initial temperature of the workpiece is considered to be surrounding temperature.

As shown in Figure 4, the wheel speed is v_s and the table speed is v_w. When the grits begin to contact the workpiece, the vertical force and elastic deformation of the workpiece is small. The grits only rub the workpiece surface. As the table is going on, the vertical force becomes larger, and the grits are pressed into the workpiece surface. Because of material plastic deformation, the bits become and the grits plough the surface. When the depth of the grits

into surface and the vertical force become much larger, the chips are cut from the surface. So there are three separate grain action: rubbing; ploughing; and cutting. At the stages of rubbing and ploughing, friction between grits and workpiece surface is the main action, and the rectangle heat flux profile is generated. At the stage of cutting, the cutting depth and the vertical force become lager and lager, which forms triangle heat flux profile. So the heat flux model should include rectangle and triangle heat flux profiles.

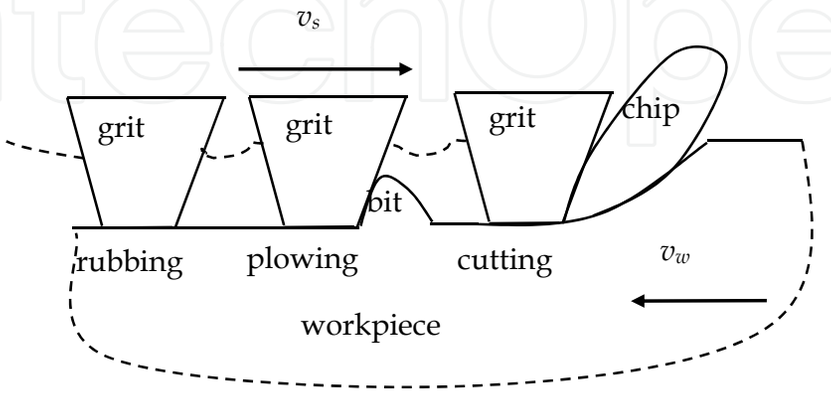

Figure 4. Grinding processes of grains

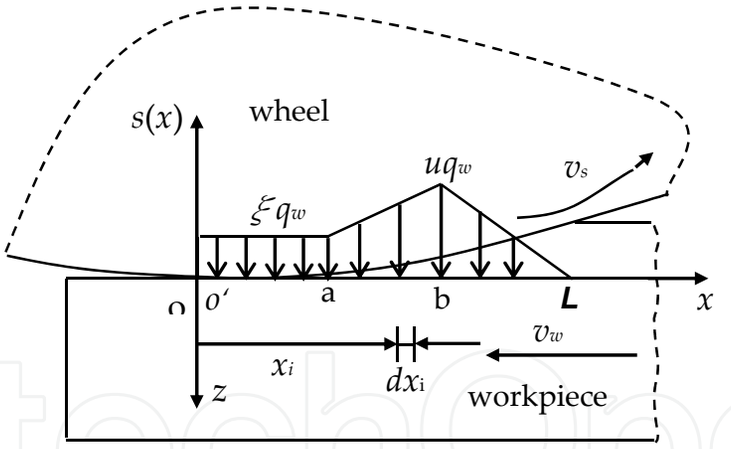

Figure 5. Heat flux profile

The coordinate system $xos(x)$ is fixed to the grinding zone with its origin o at the grinding entry point of workpiece, shown in Figure 5. The heat flux value into workpiece ξq_w is in rectangle heat flux profile and at the apex of triangle heat flux profile uq_w. The mean heat flux value q_w transfers into workpiece. The parameter ξ and u are non-dimensional parameters. The alphabet o—a is rectangle heat flux profile and the length is a. The alphabet a—L is triangle heat flux profile. The alphabet o—L is the grinding zone and the length is l_c. The alphabet b is the location of triangle heat flux apex. The length between o—b is b. The function s(x) is the grinding heat flux distribution shape function in the grinding arc and can be expressed as

$$s(x)=\begin{cases} 0 & x\in(-\infty,0) \\ \xi & x\in(0,a) \\ \dfrac{\xi(b-x)+u(x-a)}{b-a} & x\in(a,b) \\ \dfrac{u(x-L)}{b-L} & x\in(b,L) \\ 0 & x\in(L,+\infty) \end{cases} \tag{28}$$

The net heat flux per unit grinding width into the workpiece could be expressed as $q_w(x)=q_w$ s(x). The alphabet a; b; l_c; $\xi$and u is five important parameters.The contact length l_c can be calculated by wheel dimension and cutting depth. If the workpiece is harder, cutting depth is larger, table speed is higher, wheel speed is lower, and grain is bigger and sharper, cutting in the grinding process is main stage and rubbing and ploughing can be neglected. Then a=0 and ξ=0, rectriangle heat flux model becomes triangle heat flux model. If the workpiece is softer, cutting depth is smaller, table speed is lower, wheel speed is higher, and grain is smaller and duller, for example polishing, rubbing and ploughing is main stage and cutting can be neglected. Then $a=l_c$ and ξ=1, rectriangle heat flux model becomes rectangle heat flux model. The grinding fluid can reduce rubbing stage. So the alphabet a and $\xi$are related to workpiece hardness; cutting depth; table speed; wheel speed; grain and grinding fluid. Besides the above factors, the parameter b is related to grinding operations, for example up grinding and down grinding.

4.4. Thermal transfer model

The first law of thermodynamics states that thermal energy is conserved. It will be assumed that all effects are in the global Cartesian system. Specializing this to a equation as

$$\rho c\left(\frac{\partial T}{\partial t}+v_x\frac{\partial T}{\partial x}+v_y\frac{\partial T}{\partial y}+v_z\frac{\partial T}{\partial z}\right)=\bar{q}+ \\ \frac{\partial}{\partial x}\left(K_x\frac{\partial T}{\partial x}\right)+\frac{\partial}{\partial y}\left(K_x\frac{\partial T}{\partial y}\right)+\frac{\partial}{\partial z}\left(K_x\frac{\partial T}{\partial z}\right) \tag{29}$$

Where ρ-density; c-specific heat; T-temperature; t-time; K-conductivity in the element x, y, and z directions respectively; $\bar{q}$ -heat generation rate per unit volume.

Three types of boundary conditions are considered. Specified temperatures acting over surface, specified heat flows acting over surface, and specified convection surfaces acting over surface.

Dry grinding is needed in order to utilize the grinding heat in grind-hardening technology. The grinding is assumed to be quasi-stationary. The coordination system $xo'z$ is fixed to the workpiece and its origin o' is coincident with o. The width of one line heat source is defined

as dx_i, and then the heat flux value of line heat source is $q_w\, s(x_i)dx_i$. Thus the equation of the induced temperature field in the workpiece can be written as

$$T = \frac{q_w}{\pi\kappa}\int_0^{l_c} \exp\left[-\frac{(x-x_i)v_w}{2\alpha}\right] K_0\left[\frac{v_w}{2\alpha}\sqrt{(x-x_i)^2+z^2}\right] s(x_i)\,dx_i \tag{30}$$

where κ is thermal conductivity of the workpiece, α is thermal diffusivity of the workpiece, K_0 is the second order modified Bessel function.

5. Experiment set up and method

5.1. Grinding conditions

The experiment is performed on a M7120A surface grinder, using a vitrified aluminum oxide wheel (WA60L6V). The workpiece material is alloy steel 40Cr. Its chemical composition and thermal properties are listed in Table 1 and Table 2.

Material	Chemical composition of the material [%]					
	C	Si	Mn	P	S	Cr
40Cr	0.41	0.28	0.61	0.019	0.01	1.02

Table 1. Workmaterial and its chemical composition

Density	Thermal conductivity	Specific heat capacity
ρ [kg/m^3]	k [W/m·ºC]	C [J/kg·ºC]
7850	Figure 6 (a)	Figure 6 (b)

Table 2. Thermal properties of workmaterial

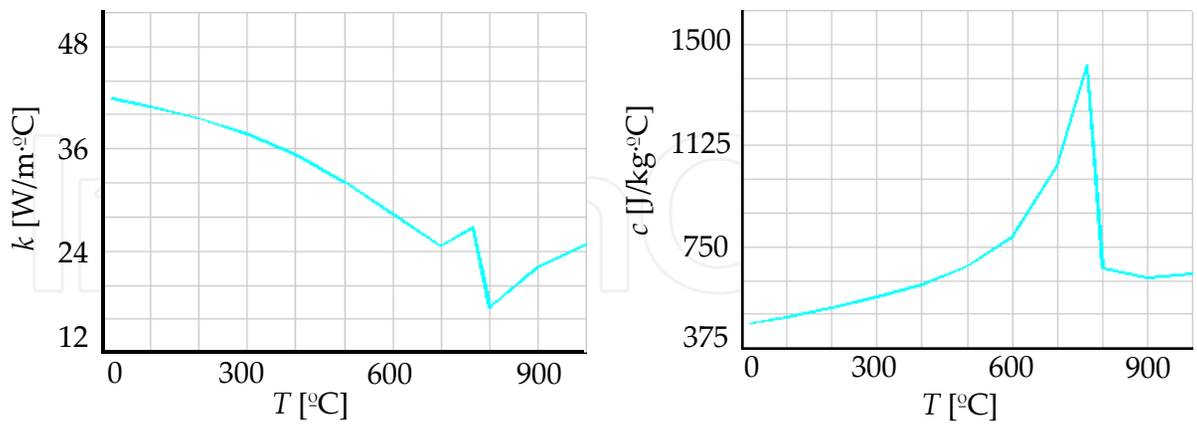

(a) thermal conductivity (b) specific heat capacity

Figure 6. Thermal properties of 40Cr steel

Grinding conditions are listed in Table 3. The work piece is fixed in a clamp in advance and is then fixed on the dynamometer. The single-point diamond dresser is used to dress the grinding wheel.

Grinding conditions	Parameters
Wheel Diameter	250[mm]
Wheel speed	35[m/s]
Table speed	0.01, 0.03 and 0.05[m/s]
Depth of cut	0.3[mm]
Coolant	Dry
Grinding operation	Down-grinding

Table 3. Grinding conditions of surface grinding

5.2. Measurement methods

A three-component dynamometer of type YDXM-III97 is used to measure the grinding forces. The dynamometer is connected to a charge amplifier of type JY5002, and the electric potential signals are converted into digital signals by an analogue-to-digital transition board of type NI 6024E, then digital signals are transferred to computer, as shown in Figure 7.

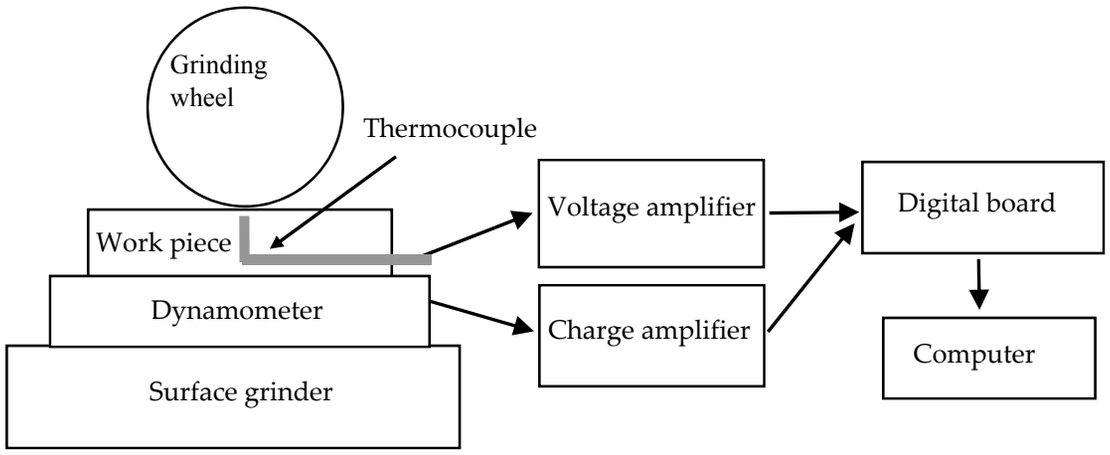

Figure 7. Schematic diagram of grind-hardening experiment

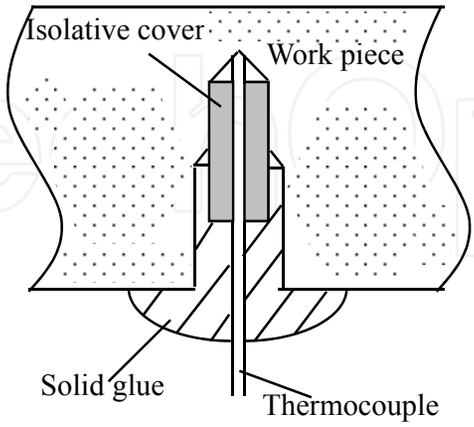

Figure 8. Schematic diagram of the thermocouple

A traditional static temperature calibration method is used in the experiment. The terminal-strand thermocouple comprising a constantan wire and an iron wire is used to measure the

temperature. The standard thermocouple and the one waiting for calibration are put in a tube furnace. The thermo-electromotive force between the standard thermocouple and the other one is measured by a potentiometer. By means of the measured temperature of the standard thermocouple the temperature in the furnace is found. Using the measured thermo-electromotive force as a reference, the thermo-electricity curve of the thermo-couple that needs to be calibrated can be described.

The thermocouple comprises a constantan wire and a threadlike chip. The constantan wire is fixed to the isolative cover and the isolative cover on the thermocouple is fixed in the mouth of the blind hole in order to avoid movement of the constantan wire. The Schematic diagram of the thermocouple is shown in Figure 8.

A traditional static temperature calibration method is used before experiment. The standard thermocouple and the one waiting for calibration are put in a tube furnace. A potentiometer measures the thermo-electromotive force between the standard thermocouple and the calibrating one. By means of the measured temperature of the standard thermocouple, the temperature in the furnace is found. Using the measured thermo-electromotive force as a reference, the thermal-electricity curve of the thermocouple need to be calibrated is described. Figure 9 is the calibration method of the thermocouple. Two terminals on the thermocouple wires are connected to the amplifier of type NI SCXI-1102, and the electric potential signals are converted into digital signals by an analogue to digital transition board of type NI 6024E. A computer records the grinding force and temperature results.

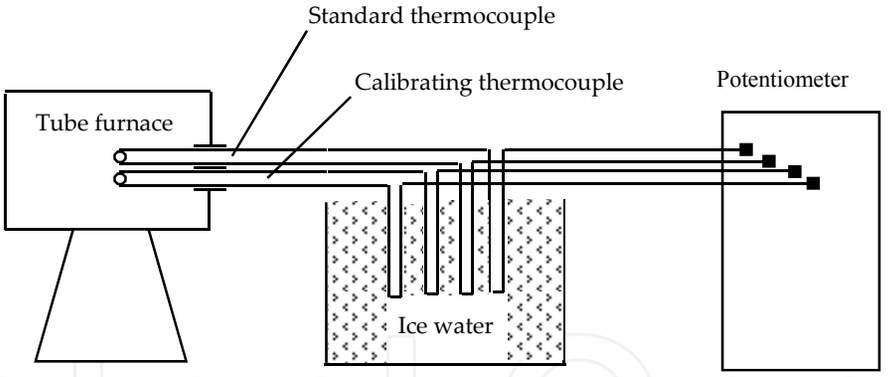

Figure 9. Calibration method of the thermocouple

6. Result and discussion

6.1. Grinding temperature field

The whole temperature field in the grinding process is shown in figure 10. The temperature gradient of work piece surface layer in grind-hardening is similar to the one in high-frequency quenching.

The comparisons between simulated temperature history obtained from the finite element model and experimental measurement reveal good agreement, as shown in Figure 11 (a), (b) and (c). The cooling rates derived from the simulated temperature history are higher than the critical cooling rate of the 40Cr steel phase transformation.

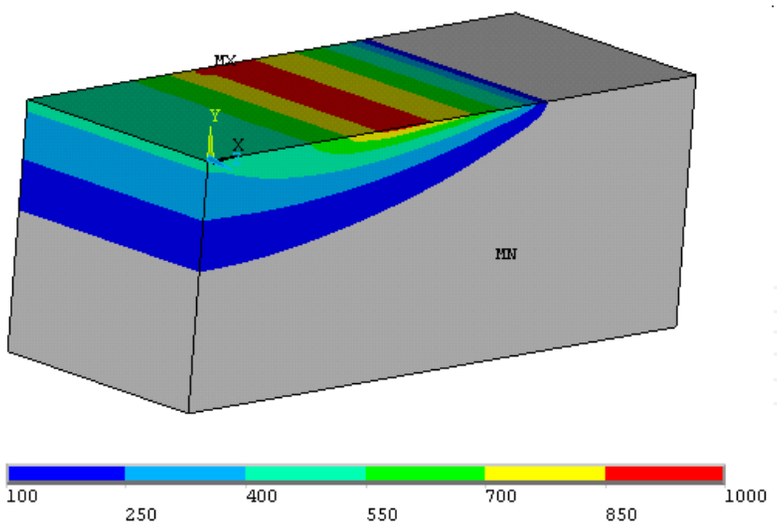

Figure 10. Grinding temperature field of workpiece

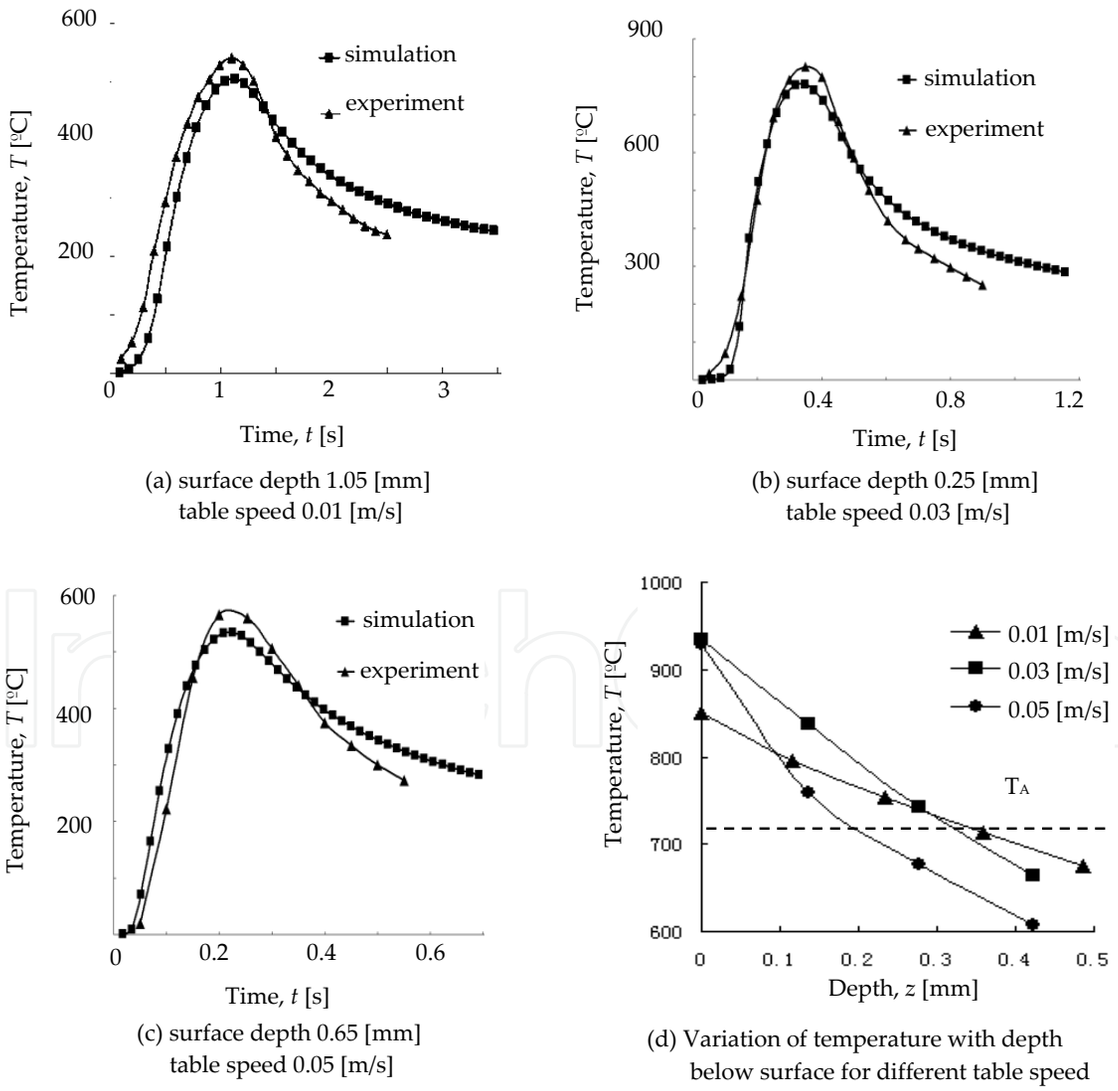

Figure 11. Comparison between simulation and experiment

The variation of the temperature in the work piece with the depth below the surface of the 40Cr steel is presented in Figure 11 (d) for table speed 0.01 m/s, 0.03 m/s and 0.05 m/s. In the figure, the critical temperature TA of austenitic transformation is indicated. Theoretically, the depth of austenitic transformation can be determined by this critical temperature. The maximum temperature of the work piece surface and the thermal gradient with the depth is down when the table speed is slow, but the hardness depth is deeper. When table speed changes from 0.05 m/s to 0.01 m/s, the hardness depth varies from 0.2 mm to 0.36 mm.

6.2. Energy partition

The temperature history underneath the ground surface of the workpiece was accurately measured by using the semi-natural thermocouple method. The theoretical values of temperature history calculated by using FEM and the experimental values of temperature history are compared in Fig. 12.

The experimental values are in qualitative agreement with the theoretical ones. An example is presented to illustrate energy partition variation along the grinding zone. The calculated energy partition distribution is shown in Fig. 13 under grinding conditions. It can be seen that the energy partition distribution deviates significantly from the traditional constant energy partition value. The energy partition within workpiece decreases from the leading edge to the trailing edge of the grinding zone, however energy partition within grinding wheel increases.

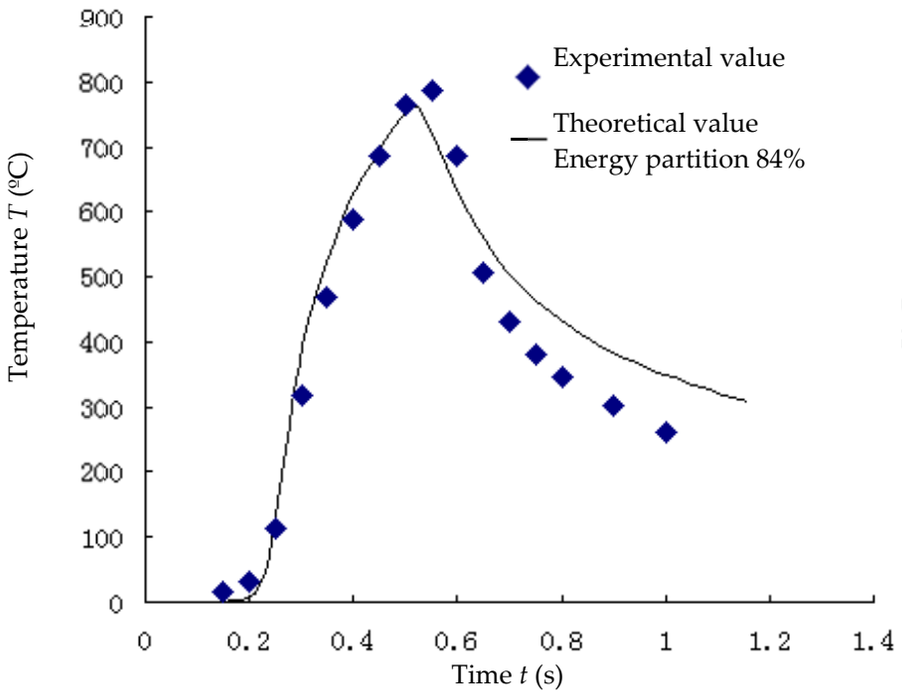

Figure 12. Compare theoretical value with experimental value of temperature history

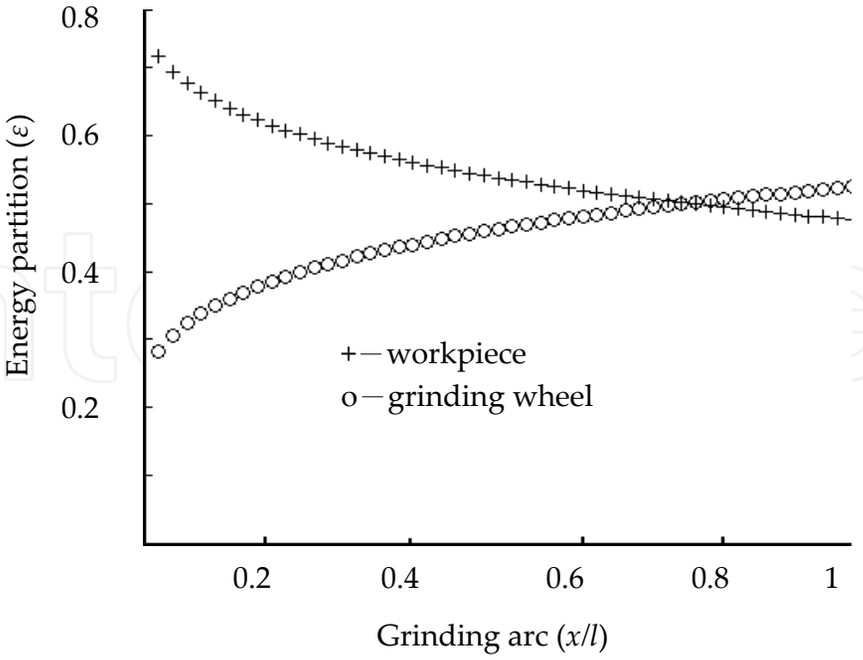

Figure 13. Energy partition within workpiece and wheel along the grinding arc zone

7. Conclusion

The finite element method was used to calculate the temperature field, maximal surface temperature and temperature history development in grind-hardening. The experiment and measurements were performed with aluminium oxide grinding wheel in different grinding conditions by using the semi-natural thermocouple method.

The austenitic and martensitic transformation layer depth of the workpiece can be predicted by the temperature history development calculated from the finite element model, the critical temperature of austenitic transformation and the critical cooling rate of martensitic transformation.

The maximum surface temperature and the thermal gradient values are lower when the table speed is slower, but the hardness depth is deeper. When table speed varies from 0.05 m/s to 0.01 m/s, the hardness depth varies from 0.2 mm to 0.36 mm.

Author details

Lei Zhang
School of Mechanical Engineering, Shandong University, P.R. China

Acknowledgement

The authors wish to thank the National Science Foundation of NSFC for financial support to the project.

8. References

Lei Zhang, Peiqi Ge and et al. 2011. Experiment and Simulation on Residual Stress of Surface Hardened Layer in Grind-Hardening. *Solid State Phenomena*. Vol. 175, pp. 166-170.

Lei Zhang and Jianlong Zhang. 2011. Temperature Measurement and Simulation in Surface Grinding. *IEEE 3rd International Conference on Computer and Network Technology*. Vols.2, pp. 589-592.

Zhang, L. and Ge, P.Q., 2004. Temperature field analysis and phase transformation research in grind-hardening. *Tool Engineering*, 38, pp. 15-19.

Brinksmeier, E. and Brockhoff, T., 1996. Utilization of grinding heat as a new heat treatment process. *Annals of the CIRP*., 45, pp. 283-286.

Brockhoff, T., 1999. Grind-hardening: A comprehensive view. *Annals of the CIRP*., 48, pp. 255-260.

Zarudi, I. and Zhang, L.C., 2002. A revisit to some wheel-workpiece interaction problems in surface grinding. *J. Mach. Tools. Manu*., 42, pp. 905-913

Zarudi, I. and Zhang, L.C., 2002. Mechanical property improvement of quenchable steel by grinding. *J. Mat. Sci.*, 37, pp. 3935-3943

Zarudi, I. and Zhang, L.C., 2002. Modeling the structure changes in quenchable steel subjected to grinding. *J. Mat. Sci*., 37, pp. 4333-4341

Wang, G.C. and Liu, J.D., 2005. Study on forming mechanism of surface hardening in two-pass grinding 40Cr steel. *Key. Eng. Mat*., 304-305,pp. 588-592

Liu, J.D. and Wang, G.C., 2004. Effect of original structure on the grind-hardened layer of 40Cr steel. *Heat Treatment of Metals*, 38, pp. 61-65

Rowe, W.B. and Jin, T., 2001. Temperature in high efficiency deep grinding. *Annals of the CIRP*., 50, pp. 205-208.

Ioan D. Marinescu, W. Brian Rowe, Boris Dimitrov and Ichiro Inasaki, 2004. Tribaology of Abrasive Machining Processes. *William Andrew publishing*.

Ramesh, M.V., Seetharamu, K.N. and Ganesan, N., 1999. Finite element modelling of heat transfer analysis in machining of isotropic materials. *Int. J. Heat. Mat. Trans*., 42, pp. 1569-1583.

Lavine, A.S., 2000. An exact solution for surface temperature in down grinding. *Int. J. Heat. Mat. Trans*., 43, pp. 4447-4456.

Zhang, L. and Ge, P.Q., 2004. New heat flux model in surface grinding. *Mat. Sci. Forum*., 471-472, pp. 298-301.

L. Zhang, P.Q. Ge, and et al. 2007. Experimental and simulation studies on temperature field of 40Cr steel surface layer in grind-hardening, *International Journal of Abrasive Technology*, Vol. 1, pp. 187-197

Lei Zhang, Wenbo Bi and et al. 2010. An Approximate Solution of Energy Partition in Grind-hardening Process. *Advanced Materials Research*. Vol. 135, pp. 298-302

Lei Zhang, and et al. 2010. Analysis of Grinding Parameters on Hardness Layer Depth. *Applied Mechanics and Materials*. Vols. 37-38, pp. 131-134